JNeurosci
THE JOURNAL OF NEUROSCIENCE

Research Articles: Systems/Circuits

Both Corticospinal and Reticulospinal Tracts Control Force of Contraction

https://doi.org/10.1523/JNEUROSCI.0627-21.2022

Cite as: J. Neurosci 2022; 10.1523/JNEUROSCI.0627-21.2022

Received: 23 March 2021
Revised: 15 December 2021
Accepted: 4 February 2022

This Early Release article has been peer-reviewed and accepted, but has not been through the composition and copyediting processes. The final version may differ slightly in style or formatting and will contain links to any extended data.

Alerts: Sign up at www.jneurosci.org/alerts to receive customized email alerts when the fully formatted version of this article is published.

Copyright © 2022 the authors

JNeurosci Accepted Manuscript

JNeurosci Accepted Manuscript

Both Corticospinal and Reticulospinal Tracts Control Force of Contraction

Isabel S Glover and Stuart N Baker

Medical School, Newcastle University, Newcastle upon Tyne, NE2 4HH, UK.

Proof and correspondence to:

Prof. Stuart Baker
Henry Wellcome Building, The Medical School, Framlington Place,
Newcastle upon Tyne, NE2 4HH, UK.
Email: stuart.baker@ncl.ac.uk

Resubmitted to *Journal of Neuroscience*

Abbreviated title: Corticospinal and reticulospinal coding of force

Conflict of Interest: The authors declare no competing financial interests.

Acknowledgements: We thank Terri Jackson for animal training; Norman Charlton for mechanical engineering; Kathy Murphy and Chris Blau for expert veterinary and anesthetic assistance; Jennifer Murray and Denise Reed for theater support; and Ashley Waddle for animal care.

Funding: This research was funded by the Reece Foundation (scholarship to I.S.G).

Number of pages: 44
Number of figures: 8
Abstract word count: 249
Introduction word count: 611
Discussion word count: 1806

JNeurosci Accepted Manuscript

27 ## Abstract

28 The control of contraction strength is a key part of movement control. In primates, both
29 corticospinal and reticulospinal cells provide input to motoneurons. Corticospinal discharge is
30 known to correlate with force, but there are no previous reports of how reticular formation (RF)
31 activity modulates with different contractions. Here we trained two female macaque monkeys
32 (body weight 5.9-6.9kg) to pull a handle which could be loaded with 0.5-6kg weights, and
33 recorded from identified pyramidal tract neurons (PTNs) in primary motor cortex and RF cells
34 during task performance. Population-averaged firing rate increased monotonically with higher
35 force for the RF, but showed a complex profile with little net modulation for PTNs. This
36 reflected a more heterogeneous profile of rate modulation across the PTN population, leading to
37 cancellation in the average. Linear discriminant analysis (LDA) classified the force based on the
38 time course of rate modulation equally well for PTNs and RF cells. Peak firing rate had
39 significant linear correlation with force for 43/92 (46.7%) PTNs and 21/46 (43.5%) RF cells. For
40 almost all (20/21) RF cells the correlation coefficient was positive; similar numbers of PTNs (22
41 vs 21) had positive vs negative coefficients. Considering the timing of force representation,
42 similar fractions (PTNs: 61.2%; RF cells: 55.5%) commenced coding before the onset of muscle
43 activity. We conclude that both corticospinal and reticulospinal tracts contribute to control of
44 contraction force; the reticulospinal tract seems to specify an overall signal simply related to
45 force, whereas corticospinal cell activity would be better suited for fine-scale adjustments.

46

47

JNeurosci Accepted Manuscript

48 ## Significance statement

49 For the first time, we compare coding of force for corticospinal and reticular formation cells in
50 awake behaving monkeys, over a wide range of contraction strengths likely to come close to
51 maximum voluntary contraction. Both cortical and brainstem systems coded similarly well for
52 force, but whereas reticular formation cells carried a simple uniform signal, corticospinal
53 neurons were more heterogenous. This may reflect a role in gross specification of a coordinated
54 movement, versus more fine-grained adjustments around individual joints.

55

JNeurosci Accepted Manuscript

Introduction

Movements occur when muscles exert forces on limbs; the control of contraction force is thus fundamental to the control of movement. Increases in force are achieved by recruitment of additional motoneurons within the pool projecting to a muscle, and also by modulating the rate of firing of motoneurons already recruited (Milner-Brown et al., 1973; Burke, 1981; Enoka and Duchateau, 2017). Increases in both rate and recruitment result from raised synaptic drive to motoneurons (Fuglevand et al., 1993). Many descending and segmental systems provide synaptic inputs to motoneurons; the relative contribution of these diverse circuits to modulation of force over its full range remains uncertain.

In primates, the corticospinal tract (CST) is a major source of descending motoneuronal drive. Evarts (1968, 1969) reported that identified pyramidal tract neurons (PTNs) modulated their discharge with force, both in movements against an external load and during isometric contractions. Cheney and Fetz (1980) took cell characterization further using spike triggered averaging to identify cortico-motoneuronal (CM) cells with direct projections to wrist flexor or extensor muscles. Cell firing rate during static contractions was positively correlated with wrist torque, consistent with these monosynaptic projections contributing some of the varying motoneuron drive required for force modulation. However, subsequent studies reveal more complex relationships.

In a dexterous finger movement task CM cells showed great heterogeneity, with negative as well as positive correlations to grip force (Maier et al., 1993). Corticospinal coding of force appears to be task-specific: some CM cells that are active during carefully controlled ramp-and-hold contractions are comparatively silent during ballistic movements (Cheney and Fetz, 1980).

JNeurosci Accepted Manuscript

78 Similarly, Muir and Lemon (1983) observed CM cells with higher firing rates during precision
79 grip than power grip, even though the muscle target of the CM projection showed higher EMG
80 activity during the latter. This led the authors to conclude that “during power grip their
81 motoneurons must receive synaptic excitation from sources other than the direct
82 corticomotoneuronal connections”.

83 In addition to the CST, both the rubrospinal tract (Ralston et al., 1988) and reticulospinal tract
84 (RST; Riddle et al., 2009) provide monosynaptic inputs to motoneurons in primates. Recordings
85 from rubromotoneuronal cells reveal tonic discharge that is also modulated by static torque,
86 although to a lesser extent than for CM cells (Cheney et al., 1988; Fetz et al., 1989).
87 Rubromotoneuronal firing rates may instead be better tuned to movement dynamics (Cheney et
88 al., 1988). The relationship between firing rates of RST neurons and force has not been directly
89 explored, yet there is evidence for an important role in force generation. Lawrence and Kuypers
90 (1968b) performed sequential lesions of two descending tracts. Loss of both CST and rubrospinal
91 tracts left animals with impairments mainly in fine finger movements, but they retained sufficient
92 strength to climb and run. This capacity was lost after combined CST/RST lesions (Lawrence
93 and Kuypers, 1968a), suggesting that the RST is capable of force modulation independent of
94 corticospinal or rubrospinal function. Furthermore, we have previously demonstrated adaptations
95 in projections from the RST during strength training (Glover and Baker, 2020), suggesting that
96 plastic changes in this tract underlie long-term changes in capacity for force generation.

97 An important limitation of all prior recordings of neural activity was that only relatively low
98 forces were examined. Direct data on how neural systems control higher forces are lacking.

JNeurosci Accepted Manuscript

99 This study aimed to compare the modulation of firing in the reticular formation (RF) and CST in
100 macaque monkeys trained to perform a weight-lifting task. We explored a wide range of weights;
101 the largest appeared close to the maximum of which the animals were capable. Both CST and
102 reticular cells coded for force, but with important differences in the nature of coding, which
103 suggest distinctive contributions to force control.

104 Materials & Methods

105 All animal procedures were performed under UK Home Office regulations in accordance with
106 the Animals (Scientific Procedures) Act (1986) and were approved by the Animal Welfare and
107 Research Ethics Board of Newcastle University. Experiments were conducted with two
108 chronically implanted, purpose-bred rhesus macaques (monkeys N and L; 5.9-6.9kg; both
109 female), which were housed together. On training days, food access was restricted in the home
110 cage and trials of the behavioral task were rewarded with food. On rest days and when trials fell
111 below a threshold value for two consecutive days, food was provided ad libitum. Ad libitum
112 access to water was provided at all times. Both animals were intact prior to the study, with the
113 exception of monkey N who had lost parts of two fingers on the right hand in an unrelated
114 incident.

115 *Behavioral Task*

116 The behavioral task has been described previously (Glover and Baker, 2020). Briefly, animals
117 were trained to pull a loaded handle towards the body using their right hand. Trials were self-
118 paced and successful completion marked by auditory feedback when the handle was moved at
119 least 4cm from its rest stop. Successful trials were rewarded with food and nucleus accumbens

JNeurosci Accepted Manuscript

120 stimulation (see below). A pulley system enabled weights to be attached to the handle, increasing
121 the force required to pull it.

122 Prior to this study, the animals were extensively trained on the task until they could perform 50
123 consecutive trials with at least 6kg attached to the handle (Glover and Baker, 2020). Animals
124 were head-fixed to enable single unit recordings (see below) and the left arm was held in a
125 restraint to ensure unilateral task performance.

126 ***Surgical Preparation***

127 As described previously, the animals were implanted with a headpiece, bilateral electromyogram
128 (EMG) electrodes in eight upper limb muscles (first dorsal interosseous, FDI; flexor digitorum
129 superficialis, FDS; flexorcarpi radialis, FCR; extensor digitorum communis, EDC; biceps
130 brachii; triceps brachii; pectoralis major, PM; and posterior deltoid muscles), and chronic
131 stimulating electrodes in the pyramidal tract (PT). The headpiece incorporated recording
132 chambers, allowing access to the left primary motor cortex (M1) and right RF. Unrelated to the
133 current study, the monkeys were also implanted with chronic stimulating electrodes in the medial
134 longitudinal fasciculus and cortical epidural electrodes. Full surgical and anesthesia details are
135 provided in our previous report (Glover and Baker, 2020).

136 In addition to food, stimulation of electrodes implanted in the nucleus accumbens was used as a
137 behavioral reward (Bichot et al., 2011). Monkey L had a preexisting nucleus accumbens
138 electrode implanted at the start of our previous study (for surgical details, see Glover and Baker,
139 2020). However, this became less effective over a period of several months, and so a second
140 electrode was implanted in this animal at the start of RF recordings and used successfully in

JNeurosci Accepted Manuscript

141 subsequent sessions. A nucleus accumbens electrode was also implanted in monkey N early in
142 the RF recordings, but stimulation did not appear to motivate behavior and so it was not
143 routinely used in this animal. When in use, nucleus accumbens stimulation was delivered every
144 1-3 successful trials (1.0-2.5mA biphasic pulses, 0.2ms per phase, 200Hz frequency, 200ms train
145 duration).

146 ***M1 recordings***

147 Recordings from PTNs were made via a recording chamber mounted on the headpiece above a
148 craniotomy centered over M1. Daily recording sessions were performed with platinum-iridium
149 microelectrodes (Thomas Recording, Marburg, Germany); up to 5 electrodes were loaded into an
150 Eckhorn microdrive (also Thomas Recording). The electrodes were individually advanced
151 through the dura and into the cortex until cell activity was detected; the animals were at rest
152 during this process. Following successful insertion of all electrodes into the cortex, the chamber
153 was filled with agar to stabilize the electrodes for cell identification and the subsequent recording
154 session.

155 Cells were identified as PTNs if they met two criteria: a fixed latency response to single-pulse
156 PT stimulation (biphasic pulses, 0.1ms per phase), and a constant collision interval (see Lemon,
157 1984). The threshold for response to PT stimulation, antidromic latency of this response,
158 collision interval and cell depth were noted for each cell. Only recordings from such identified
159 PTNs were considered in the analysis of M1 data.

JNeurosci Accepted Manuscript

160 ***RF recordings***

161 Following completion of the M1 recordings, the M1 chamber was sealed to reduce the risk of
162 infection, and a craniotomy was opened in the RF chamber. Daily recording sessions were
163 performed with either one or two 32-channel U-probes (Plexon Inc, Dallas, TX, USA); when two
164 electrodes were used, these were positioned 2mm apart on the anterior-posterior axis. The
165 electrodes were individually advanced through the craniotomy, towards the brainstem, using a
166 microdrive (Nan Instruments, Nazareth, Israel). The motor RF was identified based on location
167 relative to brainstem landmarks such as the abducens nucleus, and because intracerebral
168 microstimulation produced limb movements (trains of 18 biphasic pulses, 0.2ms per phase, 3ms
169 inter-stimulus intervals; isolated constant current stimulator Model 2100, AM Systems Inc,
170 Sequim, WA, USA).

171 ***Daily recording sessions***

172 Recording sessions were performed 5 days per week, and followed the same pattern for both M1
173 and RF recordings. During each daily session, the behavioral task was performed at seven
174 different force levels, defined by the weights attached to the lever: 0.5kg, 1kg, 1.5kg, 2kg, 3kg,
175 4kg and 6kg. The animals performed blocks of 10 trials at each weight, with the sequence of
176 weights pseudo-randomized within each recording session. Between each block there was a brief
177 pause during which the experimenter changed the weights on the task. Monkey N performed few
178 trials with 6kg during the RF recordings, so all 6kg RF data have been excluded from analysis
179 for this animal.

180 Waveform recordings from microelectrodes, U probes or EMG electrodes were amplified
181 (bandpass 1Hz-10kHz) and digitized at 25kHz sampling rate by miniature headstages (Intan

JNeurosci Accepted Manuscript

182 Technologies, Los Angeles, CA, USA), and stored to computer together with a signal
183 representing the position of the lever and digital markers indicating task events.

184 ***Data analysis***

185 The aim of this study was to compare the firing rates of PTNs and RF cells across a range of
186 weights during a weight-lifting task. All analyses were performed offline using custom scripts in
187 MATLAB, and were conducted separately for the two animals.

188 *Task Performance*

189 We started by examining measures of task performance to determine if weight was the only
190 variable that differed between trials. To achieve this, averages of lever position and rectified
191 EMG were constructed across all trials of a given weight in one session. Sweeps were aligned
192 relative to task completion (lever displacement first reaching 4cm), since this reflects the point at
193 which success was signaled to the animal. For each session, the maximum lever displacement
194 and the latency of this peak were calculated. To investigate the effect of weight on these
195 parameters, linear mixed models were constructed using single-session averages, with trial
196 weight and session ID as crossed factors. This analysis was repeated for single-session EMG
197 peak amplitude and the latency of this peak for each muscle.

198 *Spike Discrimination*

199 Waveform recordings from M1 and RF were discriminated offline into the times of single unit
200 spikes. For M1, this used custom clustering software (Getspike; S. N. Baker); spikes were only
201 included if they had consistent waveforms and inter-spike intervals >1ms. Discrimination used

JNeurosci Accepted Manuscript

202 records of spike size and shape made during the antidromic identification process, to ensure that
203 spikes corresponded to PTNs. For the RF, spikes were discriminated using MountainSort (Chung
204 et al., 2017); this software has the advantage that it can track cells that move electrode contacts
205 due to tissue instability. The MountainSort output was post-processed using custom MATLAB
206 scripts to ensure that only cells with consistent waveforms and inter-spike intervals >1ms were
207 included.

208 *Task-Related Modulation*

209 The relationship between cell firing rate and the task was examined by constructing peri-event
210 time histograms (PETHs; 10ms non-overlapping bins, smoothed by convolution with a Gaussian
211 kernel with a 20ms width parameter) relative to the task completion marker. Trials were only
212 included if the cell had an average firing rate >5Hz (measured from 1.5s before to 1s after trial
213 completion) and at least one spike in the 'active' window of the task (1s before to 0.5s after trial
214 completion); this excluded trials from periods where the cell had been lost from the record.
215 Furthermore, the first trial from each block was also excluded: for this trial, the weight was
216 unknown to the animal, which often led to the monkey producing excessive or inadequate forces,
217 depending on whether the previous block used a heavier or lighter weight. After applying these
218 trial exclusion criteria, cells were only included in the analysis if at least 5 trials per weight
219 remained for all weights, with the exception of RF recordings from monkey N for which no trials
220 were performed with the 6kg weight.

221 To determine whether the firing rate of each cell was related to task performance, a Monte Carlo
222 resampling method was used. For each trial, the inter-spike intervals were shuffled, and the
223 PETH recomputed. This randomized the spike times; on the null hypothesis that firing was

JNeurosci Accepted Manuscript

224 unmodulated by the task, shuffling should not alter the statistics of the PETH. The maximum
225 firing rate was calculated, both for the actual PETH, and after 100 different inter-spike interval
226 shuffles. For a given weight, a cell was considered significantly modulated if the real maximum
227 rate was larger than at least 95/100 of the maxima measured from shuffled PETHs. If a cell was
228 significantly modulated for all but one weight, it was considered task-modulated. Only such task-
229 modulated cells were included in the analysis.

230

JNeurosci Accepted Manuscript

231 *Linear Discriminant Analysis*

232 To assess if neural firing rate could reliably predict force, we used linear discriminant analysis
233 (LDA) to perform a pairwise classification of trials by weight. The model was trained separately
234 for each cell and each pair of weights using single trial PETHs (compiled with 100ms non-
235 overlapping bins, smoothed by convolution with a Gaussian kernel with a 100ms width
236 parameter) from 1000ms before to 500ms after task completion. LDA performance was assessed
237 with a 'leave one out' procedure in which each trial was excluded from the training set in turn,
238 and the model then used to classify the excluded trial. Accuracy was calculated as the number of
239 correctly classified trials expressed as a percentage of the total. To test if the model performed
240 significantly better than chance (50%) for each pairwise comparison, the number of correctly
241 classified trials was compared with a binomial distribution ($P<0.05$).

242 For a cell with a complete dataset of tested weights, comparisons between each pair of weights
243 produced 21 LDA accuracy values, each with an associated P value. To produce a single
244 accuracy value per cell, we averaged the LDA accuracy for all weights compared to the lightest
245 weight (0.5kg). For monkey L, this was the average of 6 values (1kg, 1.5kg, 2kg, 3kg, 4kg, 6kg
246 vs 0.5kg). For monkey N, there were only 5 values since, as described above, 6kg data was not
247 available from the RF recordings in this animal. Thus, the overall model accuracy values are
248 comparable between cell types within the same animal, but not between animals since they
249 incorporate trials at different weights. To test the overall model reliability for each cell, binomial
250 distributions were used to compare the overall model accuracy to chance (50%).

251 Several summary statistics were computed. We calculated the percentage of cells with better than
252 chance weight coding ('model reliability'), for each pair of weights compared. Similarly, by

JNeurosci Accepted Manuscript

253 averaging model accuracy for each pair of weights across all cells, we obtained an accuracy
254 value across the whole population. To limit this accuracy measure to cells in which the model
255 was reliable, we found the average model accuracy for the sub-population of cells in which
256 overall model accuracy was significantly better than chance. Finally, to provide a statistical
257 comparison between the two cell types for each monkey, we performed unpaired t-tests on
258 overall model accuracy values between PTNs and RF cells. This analysis was repeated for the
259 subpopulation of cells in which the overall model accuracy was significantly better than chance.

260 We next wanted to investigate if the peak firing rate alone could code for force. For each cell, the
261 latency of the peak firing rate was calculated from the mean PETH across all trials. A 500ms
262 window was defined centered on this latency and the maximum firing rate (10ms non-
263 overlapping bins, see above) for each trial was calculated within this window. Single trial peak
264 firing rate values were entered into the LDA model described above.

265 *Correlation of Firing Rate with Force*

266 LDA provides valuable insight into the extent to which firing rate codes for force, but it does not
267 describe the nature of this coding; for example, whether there is a positive or negative correlation.
268 To explore the relationship between peak firing rate and force further, we identified the weight
269 associated with the highest peak firing rate for each cell, and the latency at which this peak
270 occurred, relative to task completion. The distribution of peak firing rate latencies was tested for
271 normality using Kolmogorov-Smirnov tests.

272 Furthermore, for each cell we fitted a linear regression between mean peak firing rates and trial
273 weight. The gradient and significance of the peak firing rate vs force correlation was recorded for

JNeurosci Accepted Manuscript

274 each cell. Cells were classified depending on whether they had a significant positive correlation,
275 a significant negative correlation, or no correlation. We compared the gradient of the rate vs
276 force correlation between PTNs and RF cells, and between PTNs with positive and negative
277 correlations, using unpaired t-tests.

278 *Relation to Anatomical Location, and Conduction Velocity of PTNs*

279 We recorded PTNs with a range of antidromic latencies and from a range of depths. Anatomical
280 and electrophysiological studies have revealed that fast-conducting PTNs with monosynaptic
281 CM connections originate mainly from the anterior bank of the sulcus in M1, whereas slower-
282 conducting CM cells and corticospinal cells which terminate on interneurons are found
283 throughout M1 (Rathelot and Strick, 2009; Witham et al., 2016). To investigate if there was a
284 relationship between conduction velocity and force coding in PTNs, for each animal we fitted a
285 linear regression between overall model accuracy and antidromic latency. We also fitted linear
286 regressions between peak firing rate or rate/force gradient and conduction velocity. These
287 analyses were repeated for 'superficial' (<2.5mm from first recorded cell in the penetration) and
288 'deep' (>2.5mm) PTNs. Independent t-tests were performed to compare the mean model
289 accuracy per cell between 'superficial' and 'deep' PTNs.

290 *Timing of Firing Rate Changes*

291 The next analysis aimed to compare the latency of rate changes between PTNs and RF cells. To
292 do this, it was not sufficient to align activity to task completion (as in all analysis above),
293 because muscle activity often preceded lever movement by a few hundred milliseconds. This

JNeurosci Accepted Manuscript

294 timing differed between weights, with earlier EMG onset for heavier weights (see Figure 1).
295 Instead, for analysis of timing, we re-aligned firing rates to EMG onset, as described below.

296 EMG data were high-pass filtered at 30Hz, full-wave rectified, smoothed by convolution with a
297 Gaussian (width parameter σ=5ms), and binned into 1ms non-overlapping bins. The frequent
298 presence of baseline activity meant that it was not possible to detect reliably the onset of
299 increased EMG in single trials from individual muscle recordings. Instead, an average was
300 produced for a single trial across the five EMG channels in the right arm that gave clear task-
301 related activity: IDI, FDS, triceps brachii, biceps brachii and PM. To ensure that this combined
302 EMG sweep was not dominated by a single channel, each channel was first normalized by
303 dividing by its mean value across all trials.

304 Given that the animals rarely sat completely still prior to each trial of the task, baseline EMG
305 activity was not defined relative to task completion but instead by finding the quietest 500ms
306 epoch across the whole sweep (1.5s before to 1s after trial completion). For each trial, EMG
307 onset was defined by working backwards from task completion to find the first time point at
308 which EMG activity dropped below threshold (one standard deviation above mean baseline
309 EMG activity). Furthermore, trials were only included if the animals were relatively still prior to
310 EMG onset. This was defined as the 500ms prior to EMG onset being below a threshold of five
311 standard deviations above mean baseline EMG activity. Therefore, fewer trials were included in
312 EMG onset-aligned PETHs than movement onset-aligned PETHs.

313 To check the validity of EMG onset-aligned PETHs, we repeated the LDA analysis previously
314 performed on movement onset-aligned data. We calculated the average model accuracy per cell

JNeurosci Accepted Manuscript

315 and used paired t-tests to compare these values to the equivalent values from movement onset-
316 aligned PETHs.

317 To investigate latency effects, firing rate was compared between weights using single trial, EMG
318 onset-aligned PETHs with 50ms non-overlapping bins (no smoothing). For each bin, the firing
319 rate for all included trials at a given weight was compared to the firing rate for all included trials
320 at the lightest weight (0.5kg) using independent t-tests. This enabled us to calculate the
321 percentage of cells at each time point and each weight that had a significantly different firing rate
322 from the lightest weight. We also identified the first time point at which a significant difference
323 in firing rate was observed relative to the lightest weight for each cell. These values were used to
324 construct cumulative density functions for each cell type and animal to estimate when the
325 population of cells started coding for force relative to EMG onset.

326 Prior to the onset of EMG activity, it can be assumed that there is no proprioceptive or cutaneous
327 feedback regarding the weight. Therefore, if firing rate before EMG onset codes for force, this
328 would suggest that firing rate is set in anticipation of the task requirement. By contrast, firing
329 rate after EMG onset is likely to be heavily modulated by afferent feedback. We compared the
330 influence of anticipation and afferent feedback by separately performing LDA with firing rates
331 500 to 0ms before EMG onset, and 0 to 500ms after EMG onset. Single trial PETHs (EMG
332 onset-aligned, 100ms non-overlapping bins, smoothed by convolution with a Gaussian kernel
333 with a 100ms width parameter) were entered into the LDA to compare each pair of weights. The
334 overall model accuracy was compared for the 'before' and 'after' conditions and between cell
335 types with a repeated measures ANOVA; where significant effects were found, post-hoc testing
336 was performed between the 'before' and 'after' conditions with paired t-tests, and between cell

JNeurosci Accepted Manuscript

337 types with unpaired t-tests. To test if the model accuracy of the cell population was better than
338 chance, for each cell type and monkey we used one-tailed t-tests to compare the distribution of
339 'before' and 'after' overall model accuracy values to chance (0.5).

340 We observed two peaks in the EMG-aligned PETHs for PTNs; an early peak around 250ms
341 before EMG onset, and a late peak around 250ms after EMG onset. To investigate the nature of
342 these two peaks, for each trial we calculated the maximum firing rate for the early peak (500 to
343 0ms before EMG onset; pre-EMG onset window described above) and the late peak (0 to 500ms
344 after EMG onset; post-EMG onset window described above). These early peak and late peak
345 values were entered separately into an LDA model. We also calculated the maximum firing rates
346 of the early and late peaks from mean PETHs per weight per cell, and calculated the linear
347 regression between early and late amplitudes for each cell.

348 Results

349 *Task performance*

350 The weight lifting task was self-paced and the lever free to move beyond the 4cm target,
351 allowing the two monkeys to adopt their own movement strategies, which varied with force. For
352 example, with light weights both animals frequently pulled the lever beyond the 4cm target,
353 whereas with the heaviest weights they were more likely to release the lever as soon as the
354 reward tone was heard. Thus, trials were of shorter duration and had smaller lever movements
355 with the heaviest weight (Figure 1A). The period up to the success tone, which was associated
356 with the greatest EMG activity, appeared consistent across the different weights.

JNeurosci Accepted Manuscript

357 There was a pronounced increase in EMG activity with increasing task load, which was observed
358 across all muscles (Figure 1B-F). This was expected, as for a larger weight the animal not only
359 had to flex the elbow more strongly, but also grip the handle more firmly to ensure a stable grasp.
360 We did not observe a clear trend between the latency of peak EMG activity and weight across
361 the different muscles, suggesting that the timing of peak EMG activity was consistent relative to
362 task completion.

363 ***Firing rate vs force***

364 From an initial dataset of 125 PTNs and 210 RF cells, we excluded 19 PTNs and 124 RF cells
365 due to having recorded activity with insufficient trials (see Methods) and a further 14 PTNs and
366 36 RF cells since their firing rates were not task modulated. This resulted in a final dataset of 65
367 PTNs and 34 RF cells from monkey N, and 27 PTNs and 16 RF cells from monkey L.

368 PETHs of firing rate relative to task completion averaged over the whole RF cell population
369 demonstrated a clear relationship between firing rate and force (Figure 1H), whereas a more
370 complex averaged firing profile was observed for PTNs (Figure 1G). This could arise because
371 RF cells showed a greater correlation between their firing rates and force, or alternatively, that
372 there was more homogeneity in RF cell response. To test this, we compiled averages of the
373 absolute change in rate at a given weight, compared to the lightest (0.5 kg) weight, with the aim
374 of preventing cancellation across a heterogenous population. Such averages showed clearer
375 gradation with force for both monkeys (Figure 2A).

376 A more quantitative comparison of the ability of unit discharge to code force was carried out
377 using LDA. For each cell, a linear model was trained to classify single trials of two different

JNeurosci Accepted Manuscript

378 weights. For each pair of weights, we obtained an accuracy level (percentage of trials correctly
379 classified), and whether this was significantly different from chance (50%).

380 Unsurprisingly, classification reliability increased as the difference between the weights
381 increased. For example, the model performed significantly better than chance in classifying
382 0.5kg vs 6kg trials for 95.4% of PTNs in monkey N, compared to just 33.8% of cells for 0.5kg vs
383 1kg trials (Figure 2B). Overall, the model performed better than chance for 89.2% PTNs and
384 76.5% RF cells for monkey N, and 96.3% PTNs and 93.8% RF cells for monkey L (Figure 2B).
385 Considering only cells where classification was significantly better than chance, there was no
386 significant difference in model accuracy between PTNs and RF cells for monkey L (Figure 2C;
387 t_{39}=1.42, p=0.163) but the model was significantly more accurate for RF cells than PTNs for
388 monkey N (Figure 2C; t_{82}=-3.31, p=0.001). By contrast, when looking at model accuracy across
389 the whole population of cells, including those with no better than chance performance (Figure
390 2D), there was no significant difference between PTN and RF cells for either monkey (Figure
391 2E). Such a measure represents a convenient summary of overall coding efficiency of a cell
392 population, since it is sensitive both to the fraction of cells which code for force (Figure 2B), and
393 also to how accurately they code (Figure 2C). These results suggest that the firing rates of PTN
394 and RF cells reliably code force to a similar extent at the whole population level. In monkey N,
395 although a smaller percentage of RF cells reliably coded for force compared to the PTNs (Figure
396 2B), force could be predicted from firing rate more accurately in these cells (Figure 2C). Note
397 than although 6kg data have been presented for monkey N PTNs, these were not included when
398 making statistical comparisons to monkey N RF cells, where no data were available at this
399 highest force level.

JNeurosci Accepted Manuscript

400 The analysis of Figure 2 performed classification using the entire time course of the PETH
401 response. To examine which component of the firing rate profile coded for force, we next
402 simplified the LDA model to include only the peak firing rate for each trial. Although we found
403 that this strategy performed better than chance in a smaller percentage of cells (Figure 3A;
404 monkey N: PTN: 64.6%, RF: 88.2%; monkey L, PTN: 59.2%, RF: 81.3%) and was less accurate
405 (Figure 3B,C), it did reveal a significant difference between PTNs and RF cells. Across the
406 whole population, the model using peak firing rate was significantly more accurate in classifying
407 trials for RF cells than PTNs in both monkeys (Figure 3D). This effect persisted in the
408 subpopulation of monkey N cells in which the model performed significantly better than chance
409 (t_{70}=-2.68, p=0.009), but not in monkey L (t_{27}=-0.82, p=0.419).

410 To investigate the relationship between peak firing rate and force in more detail, we identified
411 the weight that generated the highest peak firing rate for each cell. For PTNs in both monkeys,
412 this was evenly distributed – individual cells could show their largest rate for anywhere from the
413 lowest to the highest weight. By contrast, for RF cells the peak firing rate was often generated by
414 the heavier weights (Figure 4A). To quantify the force-rate relationship further, we fitted a linear
415 regression between peak firing rate and force for each cell, and classified cells according to
416 whether the regression was not significant, or significant with a positive or negative slope
417 (Figure 4B). Of the cells with significant regressions, the majority (20/21) of RF cells had a
418 positive force-rate relationship whilst approximately equal numbers of PTNs had positive and
419 negative correlations (22 vs 21 cells). Figure 4C shows the change in peak firing rate at a given
420 weight, compared with the previous weight, where each line represents one cell. Figure 4D
421 presents the distribution of the peak firing rate vs weight regression slope. These plots show that
422 the strength of the rate-force relationship was similar for cells with positive and negative

JNeurosci Accepted Manuscript

423 correlations (monkey N PTNs: t_{22}=1.15, p=0.263; monkey L PTNs: t_6=-0.311, p=0.766; Figure
424 4C,D), and there was no significant difference between the rate-force relationship of PTNs and
425 RF cells with positive correlations (monkey N: t_{25}=-1.90, p=0.069; monkey L: t_{13}=-0.325,
426 p=0.751; Figure 4C,D). Finally, Figure 4E plots the latency of the peak in firing rate for the
427 weight with the highest rate, for each cell. For RF cells, the latency of peak firing rate formed a
428 normal distribution (monkey N: D_{34}=0.184, p=0.178; monkey L: D_{16}=0.213, p=0.408) centered
429 just before task completion. By contrast, the latency of peak firing rate in monkey N PTNs did
430 not form a normal distribution (D_{65}=0.180, p=0.026) but instead two distinct populations – many
431 cells had a peak firing rate before task completion, but a smaller population of cells had peak
432 firing rate after task completion (Figure 4E). A similar trend was observed in monkey L PTNs,
433 although the distribution of peak firing rate latency here was not significantly different from
434 normal (D_{27}=0.173, p=0.357).

435 The results presented above suggest that the RF cell population was relatively homogeneous,
436 whereas the PTNs showed more heterogeneity. Because PTNs were identified antidromically, we
437 were able to investigate whether this heterogeneity was associated with differences in
438 corticospinal axon conduction velocity, measured by the antidromic latency (ADL, Figure 5A).
439 There was no significant correlation between LDA model accuracy (measured as in Figure 2E)
440 and ADL (Figure 5B). There was also no significant relationship between the slope of the peak
441 firing rate vs weight relationship and ADL (Figure 5C).

442 An alternative way of classifying PTNs is by the depth of the recording site (Kozelj and Baker,
443 2014), which indicates whether a cell is likely to be in the New M1 or Old M1 subdivisions of
444 Rathelot and Strick (2009). Here, we defined the border between deep and superficial PTNs at

JNeurosci Accepted Manuscript

445 2.5mm below the first recorded cells in that penetration (Figure 5D). There was no significant
446 correlation between model accuracy and PTN depth (Figure 5E), and no significant difference
447 between the model accuracy of 'superficial' vs 'deep' PTNs (monkey N: t_{63}=-0.470, p=0.640;
448 monkey L: $t_{19.7}$=-0.836, p=0.413). Similarly, there was no correlation between the peak firing
449 rate/weight slope and PTN depth (Figure 5F). These results suggest that the heterogeneity
450 observed in our PTN population cannot be explained by differences between PTN conduction
451 velocity, nor by the location of cells within the different sub-divisions of M1.

452 ***Latency effects***

453 All of the analysis described above was carried out on PETHs aligned to task completion. This
454 marks successful performance of the task goal, and allows measurement of firing rates. We were
455 also interested in examining the timing of cell firing relative to muscle activity, but as shown by
456 Figure 1, muscle activity started earlier relative to the task completion marker for heavier
457 weights. We therefore also constructed PETHs aligned to EMG onset. Figure 6A shows PETHs
458 averaged across cell populations with this alignment. We re-ran the LDA classifier, replicating
459 the analysis of Figure 2E but with this new alignment (Figure 6B), and compared the average
460 model accuracy values with those previously obtained values. LDA showed significantly worse
461 classification using EMG-onset aligned trials for PTNs (monkey N: t_{63}=3.48, p<0.001; monkey
462 L: t_{26}=2.46, p=0.021), but was not significantly different for RF cells (monkey N: t_{33}=0.642,
463 p=0.525; monkey L: t_{14}=-0.951, p=0.358). However, similarly to the finding from task
464 completion-aligned PETHs, there was no significant difference between classifier performance
465 with PTNs and RF cells for either monkey with the EMG-onset aligned trials (Figure 6B).

JNeurosci Accepted Manuscript

466 To analyze how force coding developed in time, for each cell we compared the firing rate at a
467 given moment between each weight and 0.5kg, and tested for a significant difference. Figure 6C
468 shows how coding evolved with time across the cell population, by plotting the number of cells
469 with a significant difference at each time point. For each cell, we then found the first 50ms bin in
470 which firing rate was significantly different from the 0.5kg; the distributions of these times,
471 which reflect the onset latency of force coding, are shown as cumulative distributions in Figure
472 6D. A repeated measures ANOVA revealed no significant effect of weight (monkey N:
473 $F_{4,296}$=2.03, p=0.090; monkey L: $F_{5,160}$=1.05, p=0.392) or cell type (monkey N: $F_{1,74}$=0.14,
474 p=0.710; monkey L: $F_{1,32}$=0.543, p=0.467) on the latency of the first significant change in firing
475 rate relative to trials at 0.5kg.

476 Depending on the cell class, animal and force, between 31.3 and 79.4% of cells had an onset of
477 force coding prior to the onset of EMG. Such coding must reflect an aspect of the central
478 command for movement; after EMG onset, there could also be a contribution from afferent
479 feedback. To investigate this further, we compared the ability of the LDA model to classify trials
480 using firing rates restricted to before EMG onset ('before') vs after EMG onset ('after'). LDA
481 reliability was significantly better when using 'after' firing rates compared to 'before' rates for
482 PTNs, but there was no significant difference in 'before' and 'after' model reliability for RF cells
483 (Figure 7A,E). We also compared LDA accuracy in the subpopulation of cells in which
484 classification was significantly better than chance (Figure 7B,F), and found that the LDA
485 performed significantly better with 'after' firing rates compared to 'before' for both cell types, in
486 both animals When we repeated this analysis including all cells (and not just those where coding
487 was significantly better than chance), we saw the same result (monkey N: Figure 7C,D; monkey
488 L: Figure 7G,H). Despite the worse performance of the LDA with 'before' firing rates, we still

JNeurosci Accepted Manuscript

489 found classification accuracy of the cell populations to be significantly better than chance
490 (monkey N, PTN: t_{63}=13.7, p<0.001; monkey N, RF: t_{33}=11.9, p<0.001; monkey L, PTN:
491 t_{26}=9.76, p<0.001; monkey L, RF t_{14}=5.98, p<0.001).

492 We next wanted to investigate if the cell activity that occurred before and after EMG onset was
493 part of the same phenomena, or driven by different processes. In support of the latter, in monkey
494 N PTNs (Figure 6A) there were two clear peaks in the population firing rate, with one before and
495 one after EMG onset. To quantify how well these separate epochs coded for force, we re-ran the
496 LDA based on peak firing rate (Figure 3), first with single-trial peak firing rates restricted to the
497 time before EMG onset (-500 to 0ms; early peak) and then in a separate analysis after EMG
498 onset (0 to 500ms; late peak). Across both monkeys and cell types, LDA was significantly more
499 accurate in classifying trials based on rates from the late peak (Figure 8A). To investigate if peak
500 firing rate in these two periods was part of the same phenomenon, we looked at the correlation
501 between the early and late peak rate (Figure 8B). For each cell we fitted a linear regression
502 between the early and late peak rate and compared the R^2 values between cell types with
503 unpaired t-tests (Figure 8C). In monkey L, R^2 values were significantly higher for RF cells
504 compared to PTNs. This higher degree of correlation suggests, as can be appreciated from Figure
505 6A, that in RF cells the changes in firing rate that occur before and after EMG onset are part of
506 the same effect, whereas the lower degree of correlation for PTNs suggests that cells may behave
507 differently before and after EMG onset. However, we observed no significant differences
508 between PTN and RF R^2 values for monkey N.

JNeurosci Accepted Manuscript

509 # Discussion

510 The role of the CST in force coding is well established (for review, see Cheney et al., 1991).
511 PTN discharge is related primarily to force rather than displacement (Evarts, 1968, 1969;
512 Humphrey et al., 1970), and discharge rates show both positive and negative correlations with
513 force (Cheney and Fetz, 1980; Maier et al., 1993). Our findings extend this previous work to
514 high forces - our biggest load was comparable to the animal's body weight; pulling this with one
515 arm probably required a near-maximal contraction. Firing rate was a strong predictor of force;
516 approximately equal numbers of PTNs had peak firing rates positively or negatively correlated
517 with force (Figure 4B). Furthermore, in contrast to previous studies that investigated force
518 coding in isolated movements, our results reveal that PTN firing rate and force are also related
519 during a gross movement involving co-contraction of multiple upper limb muscles.

520 The RST provides both monosynaptic and disynaptic inputs to upper limb motoneurons (Riddle
521 et al., 2009), and hence is capable of modulating motoneuron firing rate to generate different
522 forces. We have previously demonstrated RST involvement in strength training (Glover and
523 Baker, 2020), indirectly implicating this pathway in force generation. In support of this, similar
524 to PTNs, we found that RF firing rate was highly predictive of force.

525 ## *Relative roles of CST and RST in force generation*

526 The observation that the firing rate of both PTNs and RF cells codes for force raises the question
527 of their relative roles. Although this could reflect redundancy in the motor system, our
528 observations highlight differences in brainstem and cortical force coding strategies.

JNeurosci Accepted Manuscript

529 When considering the complete time course of the task, firing rates of PTNs and RF cells
530 predicted force similarly. However, when analysis was limited to peak firing rates, RF cells
531 coded force better than PTNs. One interpretation is that RF cells provide a gross drive to
532 motoneurons, which can be well summarized by peak firing rate. By contrast, PTNs may play a
533 more sophisticated role, involving close modulation of rates to fine-tune movement. This can be
534 subjectively appreciated from the population-averaged PETHs (Figure 1G,H): RF rate increased
535 steadily prior to task completion, whilst PTN firing had a complex profile with multiple peaks.
536 Furthermore, of the cells with a significant rate-force correlation, approximately equal numbers
537 of PTNs showed positive and negative correlations, whilst all but one RF cells had positive
538 gradients. This again suggests a role for the RF in gross specification of force, compared to the
539 fine-tuning of movement by PTNs. This may be task-dependent: Muir and Lemon (1983)
540 reported higher firing rates during a precision grip than power grip task, even though the latter
541 activated muscles more. Similarly, in an alternating wrist flexion/extension task, PTN firing
542 modulated more when the direction of the load changed (requiring activation of different
543 muscles) than with force changes in one direction (Schmidt et al., 1975).

544 It might be argued that our task was especially suited to control by the RST as it generated
545 substantial co-contraction over multiple upper limb muscles. The CST seems most suited to
546 producing highly fractionated movements (Zaaimi et al., 2018), reflecting the limited divergence
547 of individual axonal projections to different motoneuron pools (Shinoda et al., 1981; Buys et al.,
548 1986). By contrast, the extensive collateralization of the RST (Peterson et al., 1975; Matsuyama
549 et al., 1997) makes it better suited to gross movements (Davidson and Buford, 2004, 2006; Baker
550 and Perez, 2017; Zaaimi et al., 2018). However, irrespective of the task's specific nature, high
551 force contractions typically involve substantial and unavoidable coactivation, often bilaterally

JNeurosci Accepted Manuscript

552 (Zijdewind and Kernell, 2001). A task which generated strong but isolated activation of a single
553 muscle would be impossible to implement and poorly reflect the reality of real-life high-force
554 tasks. A further limitation of our task was that contractions were brief, and did not include a
555 sustained holding phase; the neural substrates controlling sustained versus phasic contractions
556 may have important differences (Albert et al., 2020). However, CST neurons tend to reduce their
557 activity markedly during steady holding (Baker et al., 2001), suggesting that inclusion of a hold
558 phase would be unlikely to alter the balance between CST and RST seen here.

559 It is also important to consider the connections between descending neurons and motoneurons.
560 The highly phasic and brief contractions in the present study precluded identifying cells with
561 monosynaptic connections to motoneurons with spike-triggered averaging (Fetz and Cheney,
562 1980; Lemon et al., 1986). Nonetheless, it is unlikely that the PTN heterogeneity is explained
563 solely by separating into cells with monosynaptic *versus* polysynaptic projections to
564 motoneurons (Rathelot and Strick, 2009; Witham et al., 2016). A previous study examining only
565 CM cells similarly showed that PTN firing rates can correlate positively or negatively with force
566 (Maier et al., 1993). That paper reported 6/17 (39%) of correlated CM cells had negative slopes,
567 compared to 21/43 (49%) of PTNs reported here; these proportions do not differ significantly
568 (P=0.34, chi-squared test). Likewise, Griffin et al. (2015) reported that CM cells recorded in a
569 two-dimensional wrist movement task fired in preferred directions which were not necessarily
570 aligned to the direction of action of the target muscle, leading the authors to conclude that
571 individual CM cells can control a muscle not only when it is acting as an agonist, but also in
572 situations when it functions as antagonist, synergist or fixator. Additionally, we found no
573 relationship between the force/firing rate gradient and either the recorded depth or ADL of PTNs.
574 Given that fast-conducting PTNs with monosynaptic projections are predominantly found

JNeurosci Accepted Manuscript

575 superficially within M1 (Rathelot and Strick, 2009; Witham et al., 2016), we would predict
576 divergence in firing rate characteristics with these properties if PTN heterogeneity could be
577 explained by their projections. Another relevant aspect of descending connectivity is whether an
578 axon contacts inhibitory interneurons (Jankowska et al., 1968; Jankowska et al., 1976), which
579 would manifest in spike-triggered averages of EMG as a post-spike suppression (Kasser and
580 Cheney, 1985). Such cells might be expected to show negative correlations with force, although
581 as shown by Maier et al. (1993) CM cells with direct, excitatory projections to motoneurons can
582 also, unexpectedly, have negative correlations.

583 ***Force specification***

584 Our task was performed in blocks of 10 trials at the same weight. The animals typically
585 generated inappropriate force for the first trial per block, while subsequent trials were performed
586 with more control reflecting an accurate motor plan (Johansson and Westling, 1988). The first
587 trial was accordingly excluded from all analysis. Firing rates which modulate with force prior to
588 EMG onset must reflect internal storage of the required force, and a centrally-generated motor
589 command. By contrast, rate modulation after EMG onset could be generated in response to
590 sensory feedback from proprioceptive or cutaneous afferents. In that case, activity might still
591 contribute differential drive to motoneuron pools, but would not signify the causal spark which
592 ignites the specific movement.

593 To investigate these possibilities, we examined the coding of force by firing rate before and after
594 muscle activity onset. Unsurprisingly, for both PTNs and RF cells firing rate after muscles
595 became active was a better predictor of force than before. However, decoding of force from

JNeurosci Accepted Manuscript

596 firing rate was still significantly better than chance before EMG onset for both areas, suggesting
597 that force is specified prior to movement by both PTNs and RF cells.

598 The finding that force is specified in M1 prior to movement agrees with much previous work. In
599 humans, disruption of M1 by repetitive transcranial magnetic stimulation prevents subjects using
600 prior experience to generate appropriate force levels (Chouinard et al., 2005; Berner et al., 2007),
601 implying cortical involvement in weight storage. In monkeys, a small proportion of M1 neurons
602 show significant force coding prior to a reach and grasp task (Hendrix et al., 2009), supporting a
603 cortical role in force planning. Similarly, RF cells are active in the preparatory phase of a
604 reaching movement (Buford and Davidson, 2004; Schepens and Drew, 2004). Cortical
605 projections (including from M1) converge extensively onto the RF (Fisher et al., 2020); many of
606 these corticoreticular projections are PTN collaterals (Keizer and Kuypers, 1989). Force coding
607 prior to muscle activity onset in RF neurons could therefore be caused by descending instructions
608 from the cortex.

609 After movement onset, sensory feedback fine-tunes the pattern and force of muscle activity. Both
610 M1 and RF receive sensory inputs (Rosén and Asanuma, 1972; Leiras et al., 2010); feedback
611 from cutaneous and proprioceptive receptors will influence firing rates in both regions. Modern
612 conceptions of the motor program emphasize the importance of integration of sensory feedback
613 (Todorov and Jordan, 2002). Disruption of sensory feedback produces profound acute motor
614 deficits (Cole and Katifi, 1991; Darian-Smith and Ciferri, 2005), which can be characterized
615 clinically as weakness (Ng and Baker, 2021). Temporary deafferentation modifies M1 activity in
616 both monkeys (Lewis et al., 1971) and humans (Galan et al., 2015). Our finding that PTN and RF
617 firing rates can predict force both before and during movement suggests that force coding likely

JNeurosci Accepted Manuscript

618 occurs through a combination of internal storage of object weight and afferent feedback. In this
619 context, we should note that that one of the animals studied had lost part of two digits on the
620 hand in an unrelated incident prior to beginning training on the task. Results did not appear to
621 differ between this animal and the one with an intact hand, but we cannot exclude that altered
622 afferent feedback could have modified both M1 and RF activity in this monkey.

623 ***Modulation of motoneuron excitability***

624 Increased descending drive to motoneurons can modulate muscle force through recruitment of
625 additional motoneurons (Henneman, 1957) and/or increased firing rate of motoneurons (Monster
626 and Chan, 1977). Motoneurons are also regulated by spinal circuits. For example, C-boutons,
627 which provide cholinergic inputs to motoneurons (Witts et al., 2014), are likely necessary for
628 high-force outputs since their genetic inactivation reduces muscle activity (Zagoraiou et al.,
629 2009). Motoneuron gain may also be regulated by persistent inward currents, which can amplify
630 the response to synaptic inputs (Binder et al., 2020). Such mechanisms may tune motoneuron
631 responses to a given input, but are unlikely to overcome the need for descending inputs to
632 generate different forces. Indeed, descending inputs are required to configure these systems (e.g.
633 descending monoamine pathways such as the raphespinal tract, which activate persistent inward
634 currents), so that part of the impact of the rate modulation may occur via these spinal circuits,
635 rather than by a direct action on motoneurons.

636 ***Summary***

637 Firing rates of both PTNs and RF cells can predict force output. However, it is unlikely that these
638 represent identical, redundant routes for force control. The results are consistent with RF neurons
639 providing a simple gross drive to motoneurons, whilst PTNs fine tune activation according to the

640 detailed requirements of the movement. For both PTNs and RF cells, firing rates code the
641 required force output prior to activation of muscles, but also after the onset of muscle contraction,
642 when firing could be modulated by sensory feedback.

643

644

JNeurosci Accepted Manuscript

JNeurosci Accepted Manuscript

645 # References

646 Albert ST, Hadjiosif AM, Jang J, Zimnik AJ, Soteropoulos DS, Baker SN, Churchland MM,
647 Krakauer JW, Shadmehr R (2020) Postural control of arm and fingers through integration of
648 movement commands. eLife 9.

649 Baker SN, Perez MA (2017) Reticulospinal contributions to gross hand function after human
650 spinal cord injury J Neurosci 37:9778-9784.

651 Baker SN, Spinks R, Jackson A, Lemon RN (2001) Synchronization in monkey motor cortex
652 during a precision grip task. I. Task-dependent modulation in single-unit synchrony. J
653 Neurophysiol 85:869-885.

654 Berner J, Schönfeldt-Lecuona C, Nowak DA (2007) Sensorimotor memory for fingertip forces
655 during object lifting: the role of the primary motor cortex. Neuropsychologia 45:1931-1938.

656 Bichot NP, Heard MT, Desimone R (2011) Stimulation of the nucleus accumbens as behavioral
657 reward in awake behaving monkeys. J Neurosci Methods 199:265-272-272.

658 Binder MD, Powers RK, Heckman CJ (2020) Nonlinear Input-Output Functions of Motoneurons.
659 Physiology (Bethesda) 35:31-39.

660 Buford JA, Davidson AG (2004) Movement-related and preparatory activity in the reticulospinal
661 system of the monkey. Exp Brain Res 159:284-300.

662 Burke RE, ed (1981) Motor units: anatomy, physiology, and functional organization. Bethesda,
663 MD: American Physiological Society.

664 Buys EJ, Lemon RN, Mantel GWH, Muir RB (1986) Selective facilitation of different hand
665 muscles by single corticospinal neurones in the conscious monkey. J Physiol 381:529-549.

JNeurosci Accepted Manuscript

666 Cheney PD, Fetz EE (1980) Functional classes of primate corticomotoneuronal cells and their
667 relation to active force. J Neurophysiol 44:773-791-791.

668 Cheney PD, Mewes K, Fetz EE (1988) Encoding of motor parameters by corticomotoneuronal
669 (CM) and rubromotoneuronal (RM) cells producing postspike facilitation of forelimb muscles in
670 the behaving monkey. Behav Brain Res 28:181-191.

671 Cheney PD, Fetz EE, Mewes K (1991) Neural mechanisms underlying corticospinal and
672 rubrospinal control of limb movements. Prog Brain Res 87:213-252.

673 Chouinard PA, Leonard G, Paus T (2005) Role of the primary motor and dorsal premotor
674 cortices in the anticipation of forces during object lifting. J Neurosci 25:2277-2284.

675 Chung JE, Magland JF, Barnett AH, Tolosa VM, Tooker AC, Lee KY, Shah KG, Felix SH,
676 Frank LM, Greengard LF (2017) A Fully Automated Approach to Spike Sorting. Neuron
677 95:1381-1394.e1386-1394.e1386.

678 Cole JD, Katifi HA (1991) Evoked potentials in a man with a complete large myelinated fibre
679 sensory neuropathy below the neck. Electroencephalogr Clin Neurophysiol 80:103-107.

680 Darian-Smith C, Ciferri MM (2005) Loss and recovery of voluntary hand movements in the
681 macaque following a cervical dorsal rhizotomy. J Comp Neurol 491:27-45.

682 Davidson AG, Buford JA (2004) Motor Outputs From the Primate Reticular Formation to
683 Shoulder Muscles as Revealed by Stimulus-Triggered Averaging. J Neurophysiol 92:83-95-95.

684 Davidson AG, Buford JA (2006) Bilateral actions of the reticulospinal tract on arm and shoulder
685 muscles in the monkey: stimulus triggered averaging. Exp Brain Res 173:25-39-39.

686 Enoka RM, Duchateau J (2017) Rate Coding and the Control of Muscle Force. Cold Spring Harb
687 Perspect Med 7.

JNeurosci Accepted Manuscript

688 Evarts EV (1968) Relation of pyramidal tract activity to force exerted during voluntary
689 movement. J Neurophysiol 31:14-27.

690 Evarts EV (1969) Activity of pyramidal tract neurons during postural fixation. J Neurophysiol
691 32:375-385.

692 Fetz EE, Cheney PD (1980) Postspike facilitation of forelimb muscle activity by primate
693 corticomotoneuronal cells. J Neurophysiol 44:751-772.

694 Fetz EE, Cheney PD, Mewes K, Palmer S (1989) Control of forelimb muscle activity by
695 populations of corticomotoneuronal and rubromotoneuronal cells. Prog Brain Res 80:437-449.

696 Fisher KM, Zaaimi B, Edgley SA, Baker SN (2020) Extensive Cortical Convergence to Primate
697 Reticulospinal Pathways. J Neurosci.

698 Fuglevand AJ, Winter DA, Patla AE (1993) Models of recruitment and rate coding organization
699 in motor-unit pools. J Neurophysiol 70:2470-2488.

700 Galan F, Baker MR, Alter K, Baker SN (2015) Degraded EEG decoding of wrist movements in
701 absence of kinaesthetic feedback. Hum Brain Mapp 36:643-654.

702 Glover IS, Baker SN (2020) Cortical, Corticospinal, and Reticulospinal Contributions to Strength
703 Training. J Neurosci 40:5820-5832.

704 Griffin DM, Hoffman DS, Strick PL (2015) Corticomotoneuronal cells are "functionally tuned".
705 Science 350:667-670.

706 Hendrix CM, Mason CR, Ebner TJ (2009) Signaling of grasp dimension and grasp force in
707 dorsal premotor cortex and primary motor cortex neurons during reach to grasp in the monkey. J
708 Neurophysiol 102:132-145.

JNeurosci Accepted Manuscript

709 Henneman E (1957) Relation between size of neurons and their susceptibility to discharge.
710 Science 126:1345-1347.

711 Humphrey DR, Schmidt EM, Thompson WD (1970) Predicting measures of motor performance
712 from multiple cortical spike trains. Science 170:758-762.

713 Jankowska E, Padel Y, Tanaka R (1976) Disynaptic inhibition of spinal motoneurones from the
714 motor cortex in the monkey. J Physiol 258:467-487.

715 Jankowska E, Lund S, Lundberg A, Pompeiano O (1968) Inhibitory effects evoked through
716 ventral reticulospinal pathways. Arch Ital Biol 106:124-140.

717 Johansson RS, Westling G (1988) Coordinated isometric muscle commands adequately and
718 erroneously programmed for the weight during lifting task with precision grip. Exp Brain Res
719 71:59-71.

720 Kasser RJ, Cheney PD (1985) Characteristics of corticomotoneuronal post-spike facilitation and
721 reciprocal suppression of EMG activity in the monkey. J Neurophysiol 53:959-978.

722 Keizer K, Kuypers HGJM (1989) Distribution of corticospinal neurons with collaterals to the
723 lower brain stem reticular formation in monkey (Macaca fascicularis). Exp Brain Res 74:311-
724 318.

725 Kozelj S, Baker SN (2014) Different phase delays of peripheral input to primate motor cortex
726 and spinal cord promote cancellation at physiological tremor frequencies. J Neurophysiol
727 111:2001-2016.

728 Lawrence DG, Kuypers HG (1968a) The functional organization of the motor system in the
729 monkey. II. The effects of lesions of the descending brain-stem pathways. Brain : a journal of
730 neurology 91:15-36-36.

JNeurosci Accepted Manuscript

731 Lawrence DG, Kuypers HG (1968b) The functional organization of the motor system in the
732 monkey. I. The effects of bilateral pyramidal lesions. Brain : a journal of neurology 91:1-14-14.

733 Leiras R, Velo P, Martín-Cora F, Canedo A (2010) Processing afferent proprioceptive
734 information at the main cuneate nucleus of anesthetized cats. J Neurosci 30:15383-15399.

735 Lemon RN (1984) Methods for Neuronal Recording in Conscious Animals. Wiley.

736 Lemon RN, Mantel GW, Muir RB (1986) Corticospinal facilitation of hand muscles during
737 voluntary movement in the conscious monkey. J Physiol 381:497-527.

738 Lewis MM, Porter R, Horne M (1971) The effects of impairment of afferent feedback from the
739 moving limb on the natural activities of neurones in the precentral gyrus of conscious monkeys:
740 a preliminary investigation. Brain Res 32:467-473.

741 Maier MA, Bennett KM, Hepp-Reymond MC, Lemon RN (1993) Contribution of the monkey
742 corticomotoneuronal system to the control of force in precision grip. J Neurophysiol 69:772-785-
743 785.

744 Matsuyama K, Takakusaki K, Nakajima K, Mori S (1997) Multi-segmental innervation of single
745 pontine reticulospinal axons in the cervico-thoracic region of the cat: anterograde PHA-L tracing
746 study. 377.

747 Milner-Brown HS, Stein RB, Yemm R (1973) Changes in firing rate of human motor units
748 during linearly changing voluntary contractions. J Physiol 230:371-390.

749 Monster AW, Chan H (1977) Isometric force production by motor units of extensor digitorum
750 communis muscle in man. J Neurophysiol 40:1432-1443.

751 Muir RB, Lemon RN (1983) Corticospinal neurons with a special role in precision grip. Brain
752 Res 261:312-316.

JNeurosci Accepted Manuscript

753 Ng YS, Baker MR (2021) Sensory Ganglionopathy. New England Journal of Medicine 384:192.

754 Peterson BW, Maunz RA, Pitts NG, Mackel RG (1975) Patterns of projection and braching of
755 reticulospinal neurons. Exp Brain Res 23:333-351.

756 Ralston DD, Milroy AM, Holstege G (1988) Ultrastructural evidence for direct monosynaptic
757 rubrospinal connections to motoneurons in Macaca mulatta. Neurosci Lett 95:102-106.

758 Rathelot J-A, Strick PL (2009) Subdivisions of primary motor cortex based on cortico-
759 motoneuronal cells. Proceedings of the National Academy of Sciences 106:918-923-923.

760 Riddle CN, Edgley SA, Baker SN (2009) Direct and indirect connections with upper limb
761 motoneurons from the primate reticulospinal tract. J Neurosci 29:4993-4999.

762 Rosén I, Asanuma H (1972) Peripheral afferent inputs to the forelimb area of the monkey motor
763 cortex: input-output relations. Exp Brain Res 14:257-273.

764 Schepens B, Drew T (2004) Independent and Convergent Signals From the Pontomedullary
765 Reticular Formation Contribute to the Control of Posture and Movement During Reaching in the
766 Cat. J Neurophysiol 92:2217-2238-2238.

767 Schmidt EM, Jost RG, Davis KK (1975) Reexamination of the force relationship of cortical cell
768 discharge patterns with conditioned wrist movements. Brain Res 83:213-223.

769 Shinoda Y, Yokota JI, Futami T (1981) Divergent projection of individual corticospinal axons to
770 motoneurons of multiple muscles in the monkey. Neurosci Lett 23:7-12.

771 Todorov E, Jordan MI (2002) Optimal feedback control as a theory of motor coordination. Nat
772 Neurosci 5:1226-1235.

JNeurosci Accepted Manuscript

773 Witham CL, Fisher KM, Edgley SA, Baker SN (2016) Corticospinal Inputs to Primate
774 Motoneurons Innervating the Forelimb from Two Divisions of Primary Motor Cortex and Area
775 3a. J Neurosci 36:2605-2616-2616.

776 Witts EC, Zagoraiou L, Miles GB (2014) Anatomy and function of cholinergic C bouton inputs
777 to motor neurons. J Anat 224:52-60.

778 Zaaimi B, Dean LR, Baker SN (2018) Different contributions of primary motor cortex, reticular
779 formation, and spinal cord to fractionated muscle activation. J Neurophysiol 119:235-250-250.

780 Zagoraiou L, Akay T, Martin JF, Brownstone RM, Jessell TM, Miles GB (2009) A Cluster of
781 Cholinergic Premotor Interneurons Modulates Mouse Locomotor Activity. Neuron 64:645-662-
782 662.

783 Zijdewind I, Kernell D (2001) Bilateral Interactions During Contractions of Intrinsic Hand
784 Muscles. J Neurophysiol 85:1907-1913-1913.

785

786

JNeurosci Accepted Manuscript

787 # Figures Legends

788 **Figure 1. Average muscle activity and cell firing rates relative to lever movement**

789 Mean sweeps, averaged across all recording sessions for each animal (columns), shown per
790 weight (see legend) and aligned to task completion (4cm deviation of lever; black dotted line).
791 Black scale bars are 500ms. Data shown are averaged across all 36 session from monkey N (28
792 PTN, 8 RF sessions), and 21 session from monkey L (16 PTN, 5 RF sessions). ***A.*** Mean lever
793 displacement. Linear mixed models (see Methods) were constructed to assess the effect of trial
794 weight on the amplitude (monkey N: $F_{1,242}$=42.8, p<0.001; monkey L: $F_{1,145}$=71.0, p<0.001) and
795 latency (monkey N: $F_{1,242}$=59.4, p<0.001; monkey L: $F_{1,145}$=143, p<0.001) of maximum lever
796 displacement. ***B-F:*** Rectified mean EMG activity. Linear mixed models with single session data
797 were used to assess the effect of trial weight on the amplitude and latency of peak EMG activity.
798 ***B.*** First dorsal interosseous (monkey N amplitude: $F_{1,242}$=903, p<0.001; monkey N latency:
799 $F_{1,242}$=48.6, p<0.001; monkey L amplitude: $F_{1,145}$=586, p<0.001; monkey L latency: $F_{1,145}$=6.41,
800 p=0.012). ***C.*** Flexor digitorum superficialis (monkey N amplitude: $F_{1,242}$=868, p<0.001; monkey
801 N latency: $F_{1,242}$=2.00, p=0.159; monkey L amplitude: $F_{1,145}$=771, p<0.001; monkey L latency:
802 $F_{1,145}$=0.43, p=0.514). ***D.*** Triceps brachii (monkey N amplitude: $F_{1,242}$=487, p<0.001; monkey N
803 latency: $F_{1,242}$=3.69, p=0.056; monkey L amplitude: $F_{1,145}$=638, p<0.001; monkey L latency:
804 $F_{1,145}$=1.84, p=0.177). ***E.*** Biceps brachii (monkey N amplitude: $F_{1,242}$=1578, p<0.001; monkey N
805 latency: $F_{1,242}$=19.6, p<0.001; monkey L amplitude: $F_{1,145}$=1008, p<0.001; monkey L latency:
806 $F_{1,145}$=10.2, p=0.002). ***F.*** Pectoralis major (monkey N amplitude: $F_{1,242}$=1361, p<0.001; monkey
807 N latency: $F_{1,242}$=0.84, p=0.360; monkey L amplitude: $F_{1,145}$=1213, p<0.001; monkey L latency:
808 $F_{1,145}$=120, p<0.001). ***G.*** PETH for PTNs (monkey N: n=65; monkey: n=27). ***H.*** PETH for RF
809 cells (monkey N: n=34; monkey L: n=16).

JNeurosci Accepted Manuscript

810 **Figure 2. Firing rate across full task duration**

811 ***A.*** Mean absolute change in firing rate relative to trials performed with the 0.5kg weight. Sweeps
812 are aligned to task completion, and shown per cell type per animal (subplots) and per weight (see
813 legend). ***B-D:*** LDA comparing firing rates between each pair of weights, for each cell across the
814 full time-course of each trial. ***B.*** Percentage of cells in which the model correctly predicted the
815 weight of each trial significantly more often than chance (see Methods). ***C.*** Mean model
816 accuracy in the sub-population of cells in which the overall model accuracy was better than
817 chance (see Methods; monkey N PTN: n=58/65; monkey N RF: n=26/34; monkey L PTN:
818 n=26/27; monkey L RF: n=15/16). ***D.*** Mean model accuracy in all cells. ***E.*** Mean model
819 accuracy per cell type, per animal. Blue circles show mean model accuracy for individual cells.
820 Red errors bars show mean and standard deviation across the population of cells. Mean model
821 accuracy was compared between all PTNs and RF cells for each animal with independent two-
822 tailed t-tests (monkey N: $t_{50.3}$=-0.902, p=0.372; monkey L: t_{41}=1.44, p=0.157).

823

JNeurosci Accepted Manuscript

824 **Figure 3. Prediction of trial weight by peak firing rate**

825 LDA comparing the peak firing rate between each pair of weights, for each cell. See Methods for
826 calculation of peak firing rate. ***A.*** Percentage of cells in which the model correctly predicted the
827 weight of each trial significantly more often than chance (see Methods). ***B.*** Mean model
828 accuracy in the sub-population of cells in which the overall model accuracy was greater than
829 chance (see Methods; monkey N PTN: n=42/65; monkey N RF: n=30/34; monkey L PTN:
830 n=16/27; monkey L RF: n=13/16). ***C.*** Mean model accuracy in all cells. ***D.*** Mean model
831 accuracy per cell type, per animal. Blue circles show mean model accuracy for individual cells.
832 Red errors bars show mean and standard deviation across the population of cells. Mean model
833 accuracy was compared between PTNs and RF cells for each animal with independent two-tailed
834 t-tests (monkey N: t_{96}=-3.85, p<0.001; monkey L: t_{40}=-2.14, p=0.038).

835 **Figure 4. Peak firing rate**

836 ***A.*** The weight that generated the highest firing rate for each cell, expressed as a percentage of
837 cells per weight. ***B.*** Proportion of cells with a significant positive or negative correlation (see
838 legend) between peak firing rate and trial weight. ***C.*** Change in peak firing rate with weight,
839 limited to the sub-population of cells with a significant positive or negative correlation between
840 peak firing rate and trial weight. ***D.*** Histogram showing the slope of peak firing rate versus force
841 for each cell, grouped by the direction and significance of the relationship (see legend). ***E.***
842 Histogram of the latency of peak firing rate, expressed as a percentage of cells.

843 **Figure 5. PTN properties**

844 ***A.*** Histogram of antidromic latency (ADL) for PTNs, shown separately for each animal
845 (columns). ***B.*** Correlation between average LDA accuracy (see Figure 2) and ADL. Blue circles
846 represent individual cells, and the red line shows the linear regression (monkey N: R^2=0.004,

JNeurosci Accepted Manuscript

847 p=0.618; monkey L: R^2=0.004, p=0.749). ***C.*** Correlation between peak firing rate/force slope
848 (see Figure 4D) and ADL. Blue circles represent individual cells, and the red line shows the
849 linear regression (monkey N: R^2<0.001, p=0.825; monkey L: R^2=0.022, p=0.456). ***D.*** Histogram
850 of cell depth for PTNs, shown separately for each animal (columns). The red dotted line shows
851 the boundary between superficial and deep PTNs (2.5mm). ***E.*** Correlation between average
852 model accuracy (see Figure 2) and cell depth. Blue circles represent individual cells, and the red
853 line shows the linear regression (monkey N: R^2=0.001, p=0.804; monkey L: R^2=0.011, p=0.609).
854 ***F.*** Correlation between peak firing rate/force slope (see Figure 4D) and cell depth. Blue circles
855 represent individual cells, and the red line shows the linear regression (monkey N: R^2<0.001,
856 p=0.977; monkey L: R^2=0.003, p=0.766).

857 **Figure 6. EMG onset-aligned firing rate**

858 ***A.*** PETHs, averaged across all recording sessions for each animal and cell type (columns),
859 shown per weight (see legend) and aligned to EMG-onset (black dotted line, see Methods). Black
860 scale bars are 500ms. ***B.*** Mean LDA accuracy comparing firing rates between each pair of
861 weights, for each cell across the full time-course of each EMG onset-aligned trial. Blue circles
862 show mean LDA accuracy for individual cells. Red errors bars show mean and standard
863 deviation across the population of cells. Mean LDA accuracy was compared between all PTNs
864 and RF cells for each animal with independent two-tailed t-tests (monkey N: t_{96}=-1.81, p=0.074;
865 monkey L: t_{20}=-0.841, p=0.411). ***C.*** Percentage of cells with a significant change in firing rate
866 compared to trials at 0.5kg, shown per weight (see legend) and 50ms bin. Black dotted line
867 shows EMG onset. ***D.*** Cumulative distribution of the first 50ms bin with a significant difference
868 in firing rate compared to trials at 0.5kg, shown per weight (see legend). Black dotted line shows
869 EMG onset.

JNeurosci Accepted Manuscript

870 **Figure 7. Comparison of firing rate before and after EMG onset**

871 LDA comparing the firing rate between each pair of weights for each cell, performed separately
872 for firing rate before EMG onset (-500 to 0ms; columns 1 and 3) and after EMG onset (0 to
873 500ms; columns 2 and 4) for EMG onset-aligned PETHs (see Methods). Results are shown
874 separately for monkey N ***(A-D)*** and monkey L ***(E-H)***. ***A,E.*** Percentage of cells in which the
875 model correctly predicted the weight of each trial significantly more often than chance for each
876 pair of weights. McNemar's test compared the overall model reliability for each cell between the
877 'before' and 'after' condition (monkey N PTN: $p=0.020$; monkey N RF: $p=0.317$; monkey L
878 PTN: $p=0.014$; monkey L RF: $p=0.083$). ***B,F.*** Mean model accuracy in the sub-population of
879 cells in which the overall model accuracy was better than chance (monkey N PTN before:
880 n=54/65; monkey N PTN after: n=61/65; monkey N RF before: n=30/34; monkey N RF after:
881 n=28/34; monkey L PTN before: n=21/27; monkey L PTN after: n=27/27; monkey L RF before:
882 n=12/16; monkey L RF after: n=15/16). A repeated measures ANOVA compared mean model
883 accuracy between the 'before' and 'after' conditions (monkey N: $F_{1,77}=9.98$, $p=0.002$; monkey L:
884 $F_{1,31}=15.9$, $p<0.001$) and cell type (monkey N: $F_{1,77}=4.91$, $p=0.030$; monkey L: $F_{1,31}=2.85$,
885 $p=0.101$). Post-hoc testing compared mean model accuracy between the before and after periods
886 for each animal and cell type with paired two-tailed t-tests (monkey N PTN: monkey N: $t_{51}=-$
887 8.44, $p<0.001$; monkey N RF: $t_{26}=-4.82$, $p<0.001$; monkey L PTN: $t_{20}=-7.95$, $p<0.001$; monkey L
888 RF: $t_{11}=-6.45$, $p<0.001$). In monkey N, post-hoc testing compared model accuracy between cell
889 types for each period (before: $t_{77}=-2.71$, $p=0.008$; after: $t_{77}=-1.47$, $p=0.144$). ***C,G.*** Mean model
890 accuracy in all cells. ***D,H.*** Mean model accuracy per cell type and time period (before or after
891 EMG onset), for all cells. Blue lines show mean model accuracy for individual cells, before and
892 after EMG onset. Red errors bars show mean and standard deviation across the population of

JNeurosci Accepted Manuscript

893 cells. A repeated measures ANOVA compared mean model accuracy between the 'before' and
894 'after' conditions (monkey N: $F_{1,97}$=16.8, p<0.001; monkey L: $F_{1,41}$=6.94, p=0.012) and cell type
895 (monkey N: $F_{1,97}$=0.80, p=0.372; monkey L: $F_{1,41}$=1.71, p=0.199). Post-hoc testing compared
896 mean model accuracy between the before and after periods for each animal and cell type with
897 paired two-tailed t-tests (monkey N PTN: t_{64}=-9.60, p<0.001; monkey N RF: t_{33}=-3.59, p=0.001;
898 monkey L PTN: t_{26}=-9.17, p<0.001; monkey L RF: t_{15}=-5.00, p<0.001).

899 **Figure 8. Comparison of early and late peaks**

900 ***A.*** Mean LDA accuracy per cell type and time period (early or late peak). Blue lines show mean
901 model accuracy for individual cells, for peak firing rate in the early and late periods. Red errors
902 bars show mean and standard deviation across the population of cells. Mean LDA accuracy of
903 the early peak and late peak were compared for each animal and cell type with paired two-tailed
904 t-tests (monkey N PTN: t_{63}=-3.72, p<0.001; monkey N RF: t_{33}=-3.58, p=0.001; monkey L PTN:
905 t_{26}=-2.93, p=0.007; monkey L RF: t_{14}=-3.50, p=0.004). ***B.*** Correlation of peak firing rate in the
906 early and late period for each weight (see legend). Individual points show peak firing rate for
907 each weight, for each cell. ***C.*** R^2 values for the correlations between peak firing rate in the early
908 and late period for each cell. R^2 values were compared between PTNs and RF cells for each
909 monkey using unpaired t-tests (monkey N: t_{97}=-1.49, p=0.139; monkey L: t_{41}=-3.19, p=0.003).

910

JNeurosci Accepted Manuscript

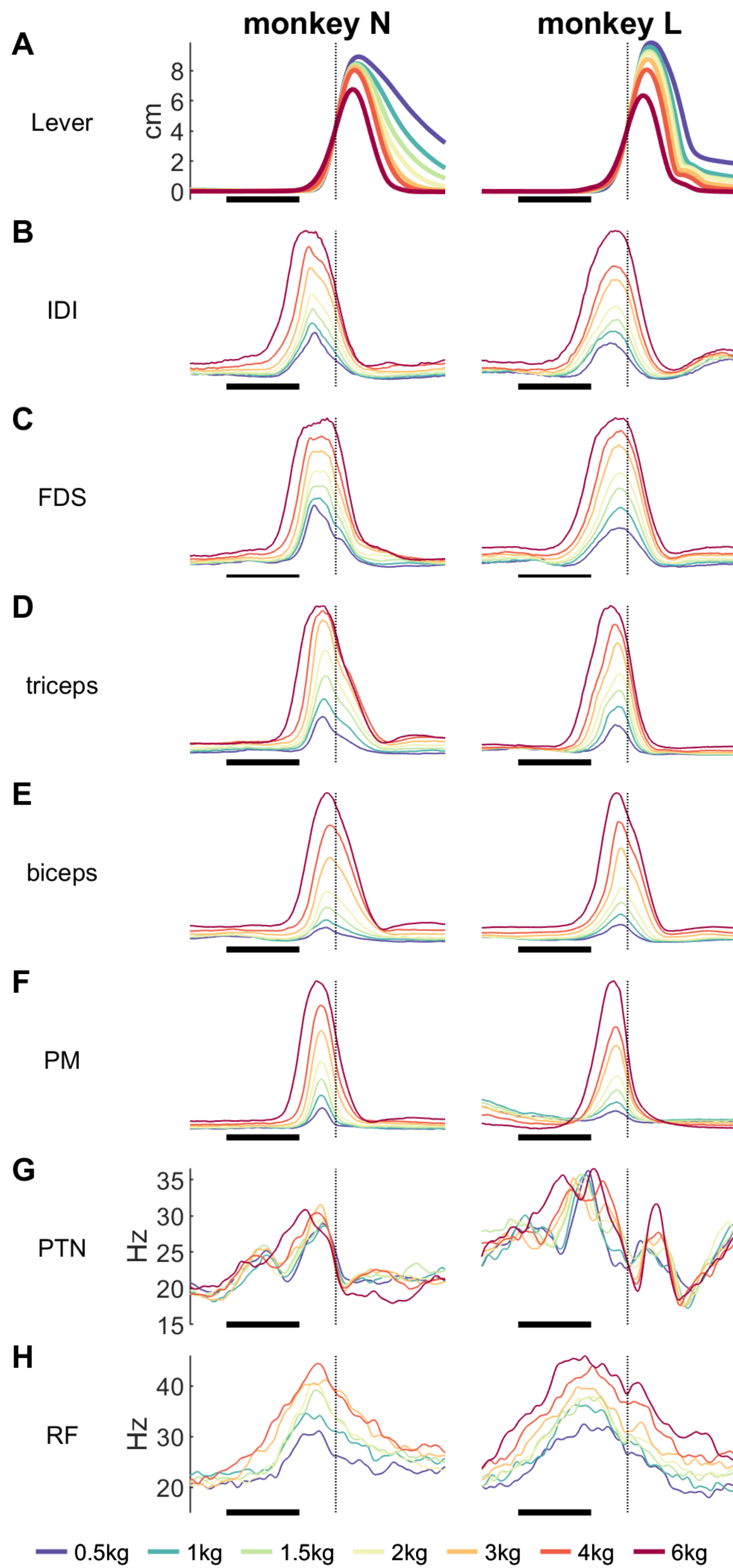

JNeurosci Accepted Manuscript

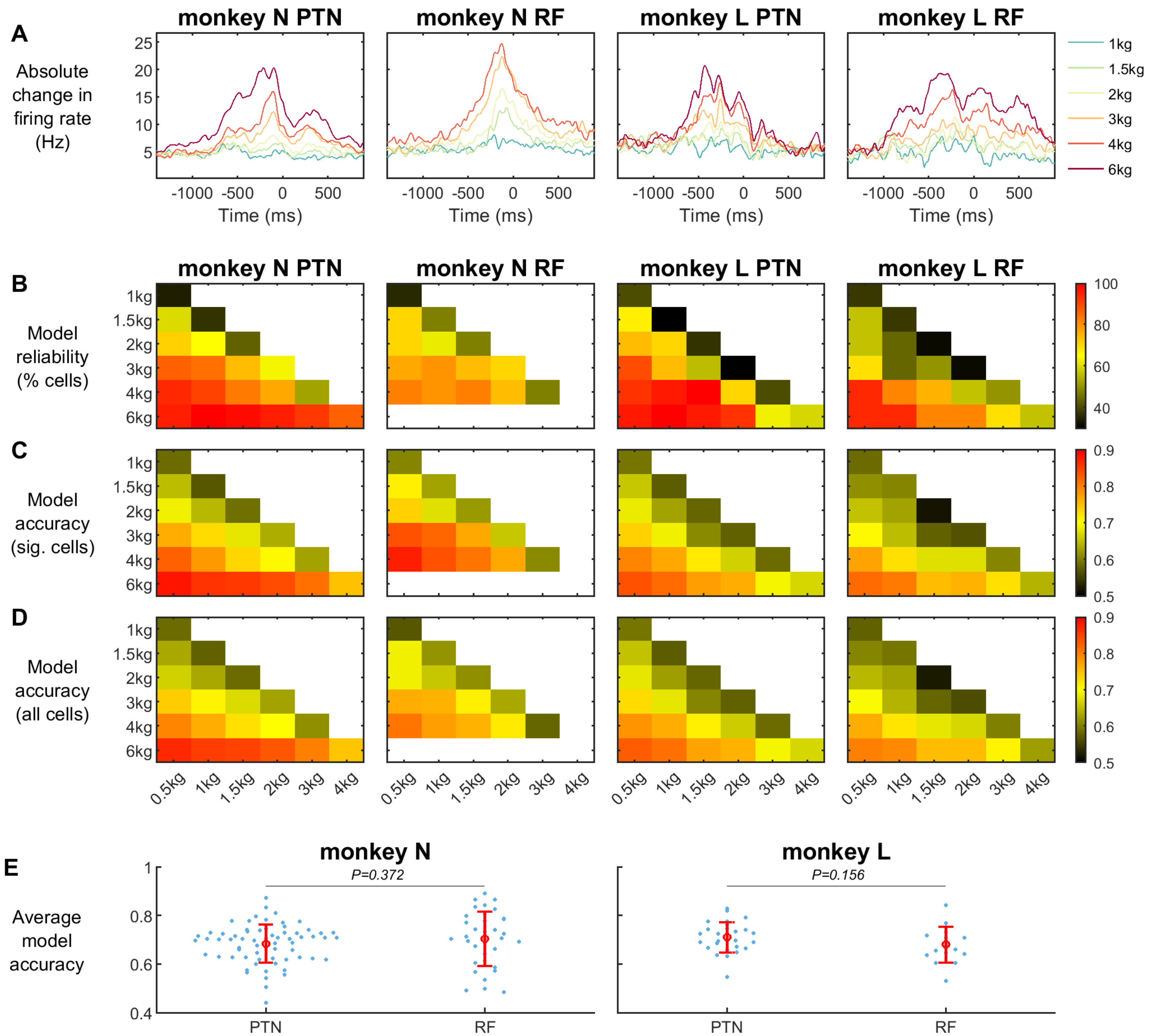

JNeurosci Accepted Manuscript

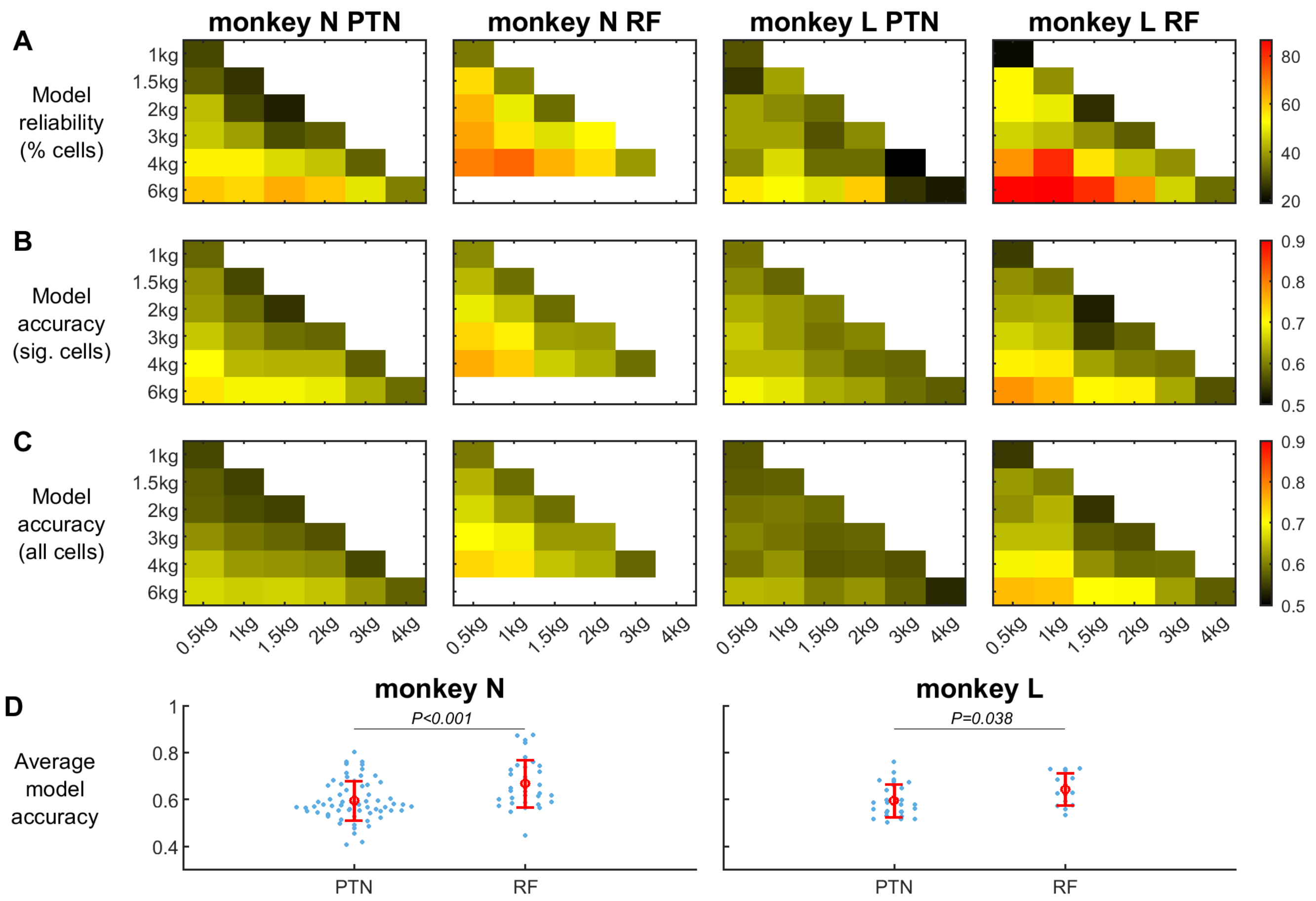

JNeurosci Accepted Manuscript

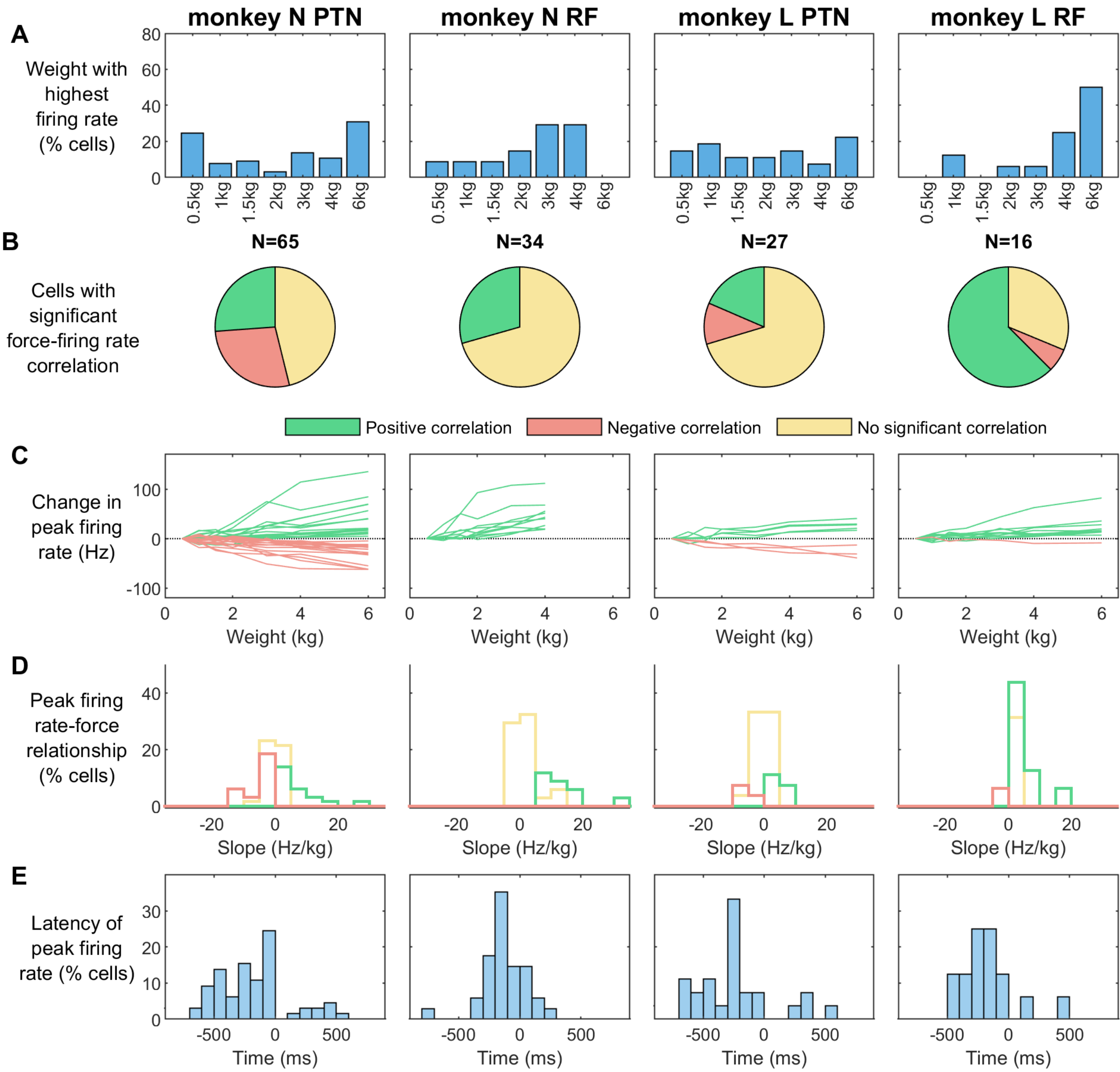

JNeurosci Accepted Manuscript

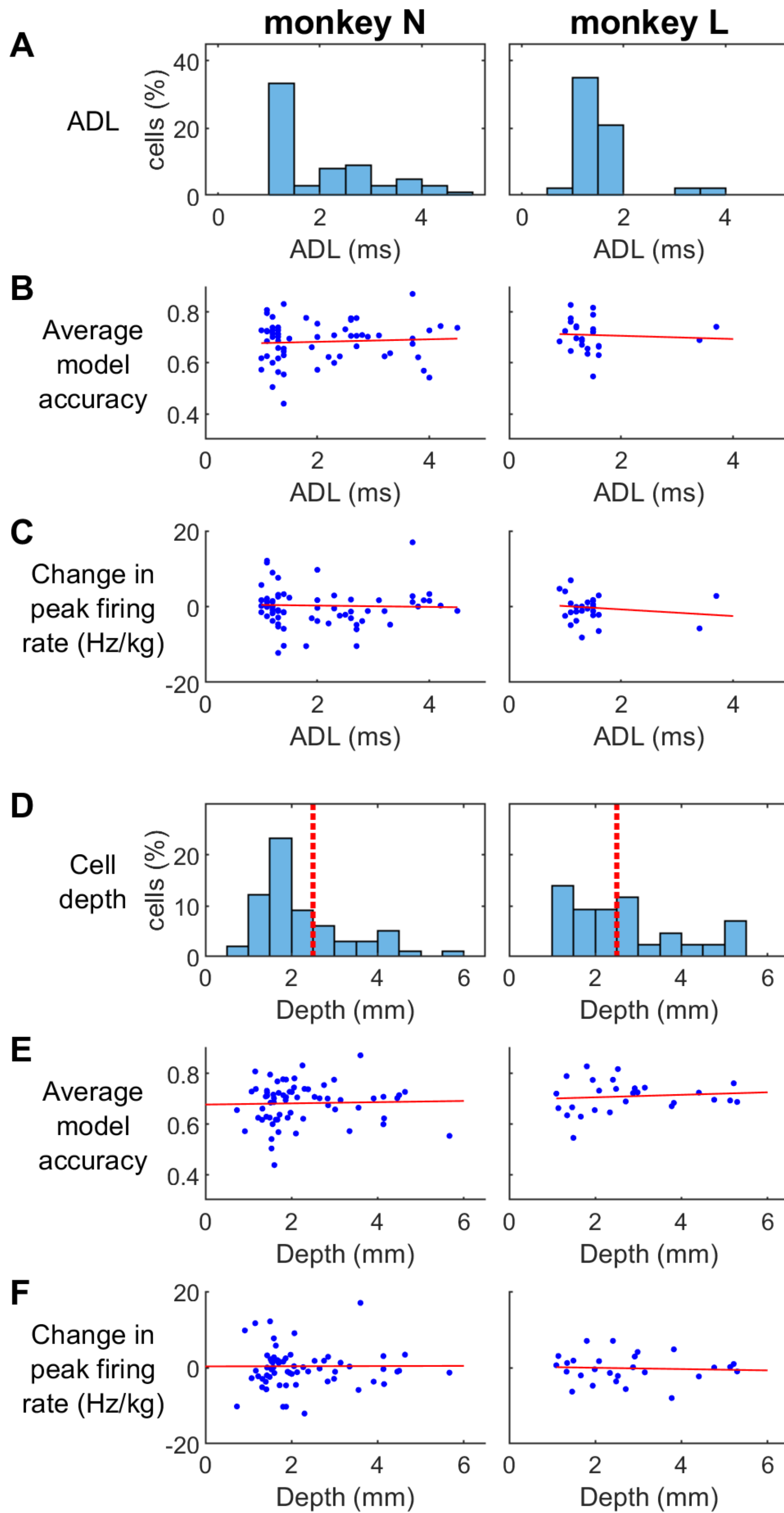

JNeurosci Accepted Manuscript

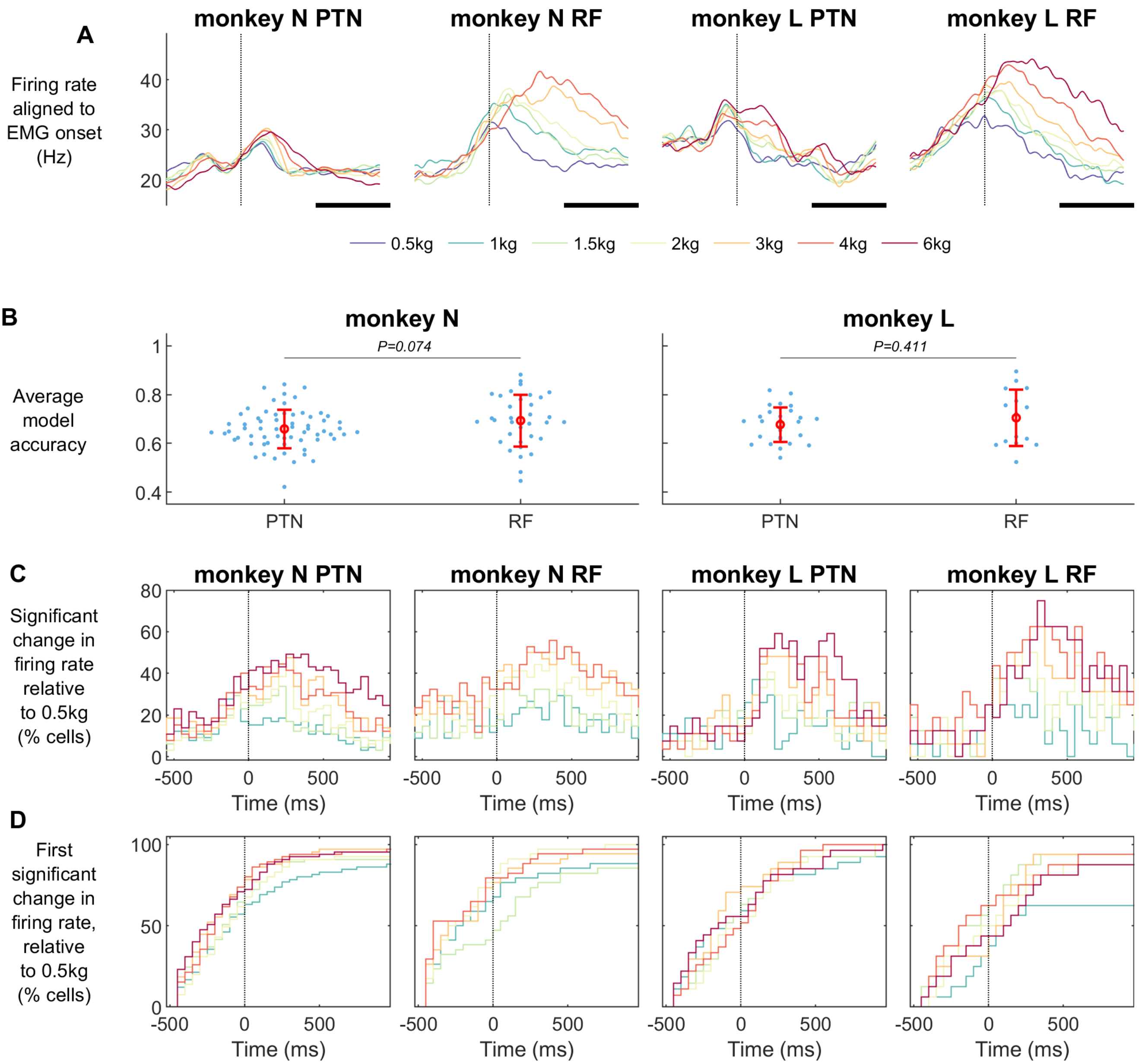

JNeurosci Accepted Manuscript

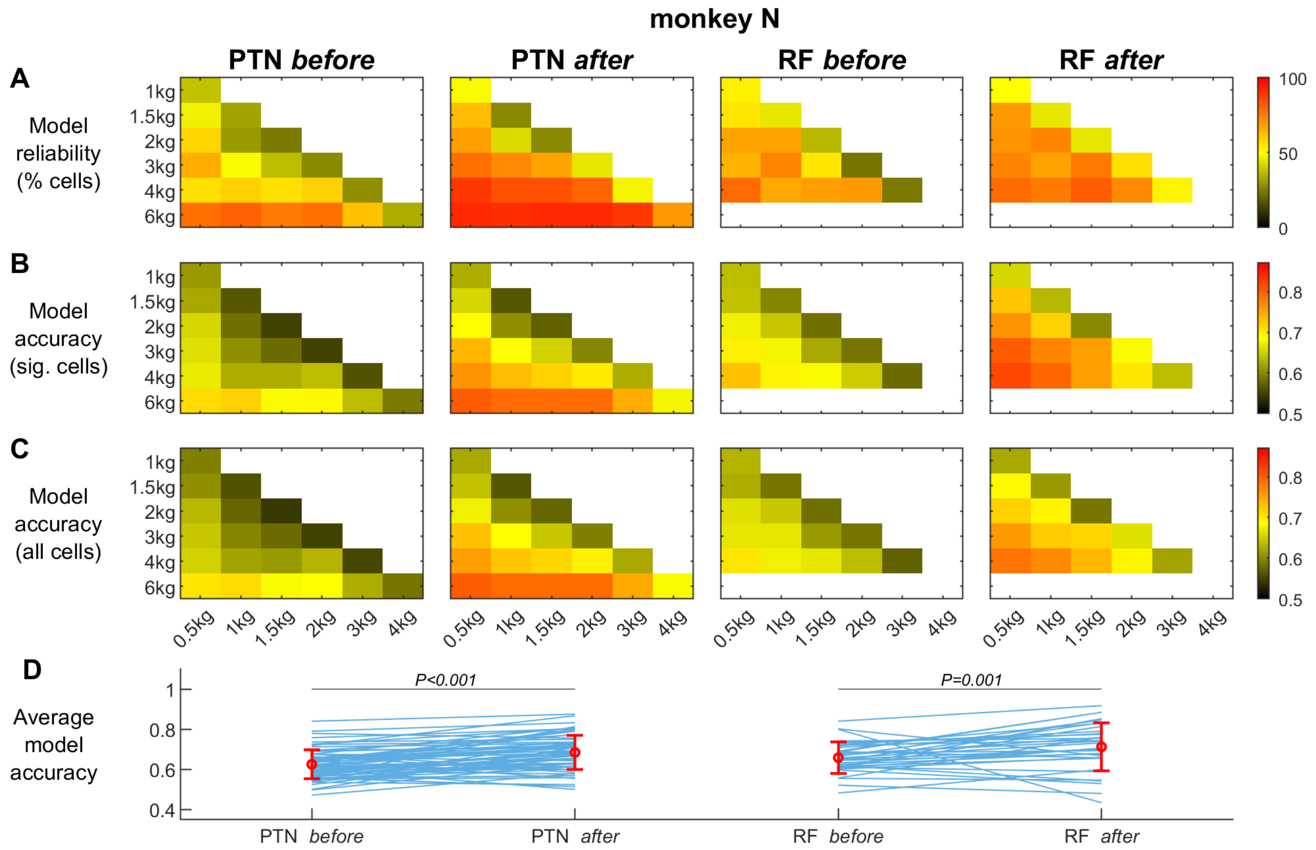

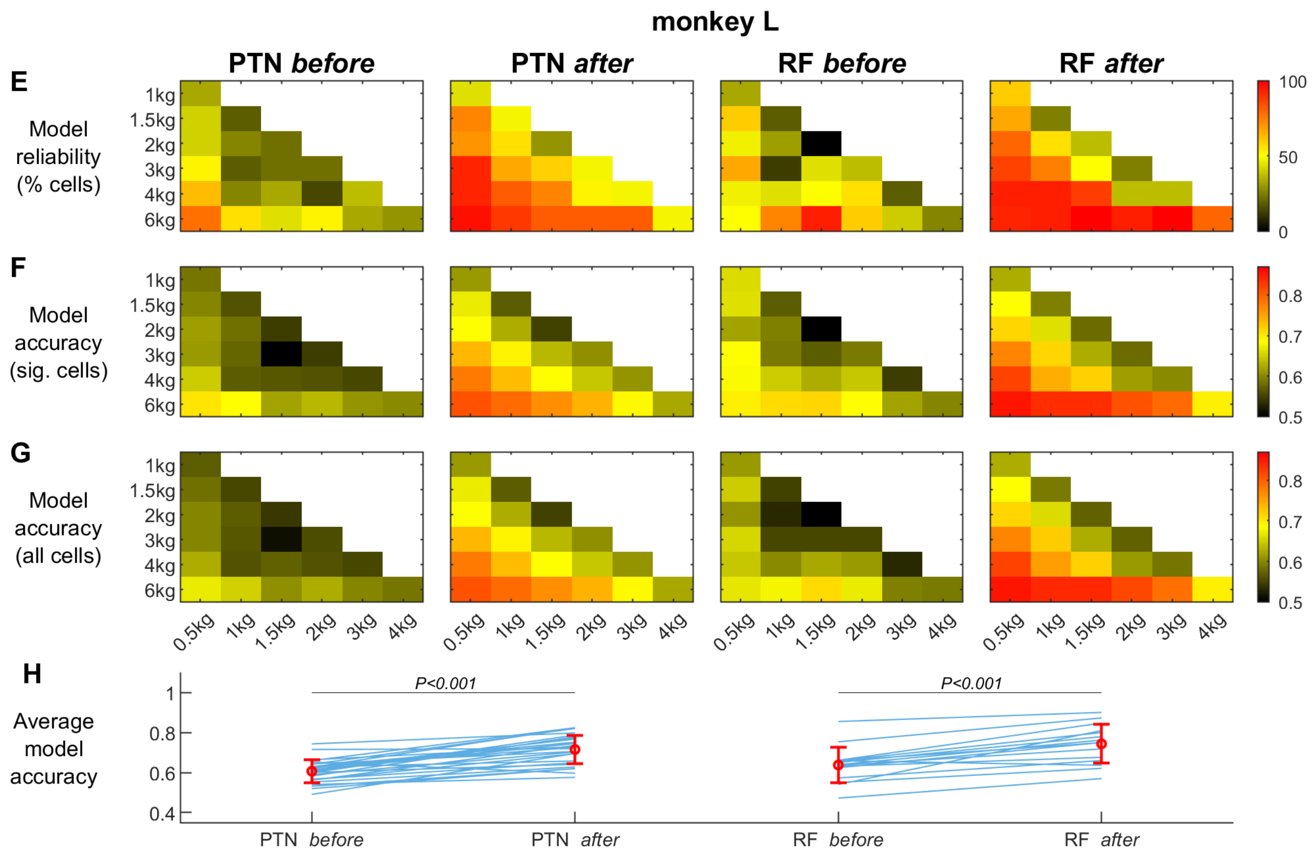

JNeurosci Accepted Manuscript